Tidal conversion at a very steep ridge

By STEFAN G. LLEWELLYN SMITH[1] AND W. R. YOUNG[2]

[1]Department of Mechanical and Aerospace Engineering, University of California, San Diego,
La Jolla CA 92093-0411, USA

[2]Scripps Institution of Oceanography, University of California, San Diego,
La Jolla CA 92093-0230, USA

We obtain an analytic solution for the generation of internal gravity waves by tidal flow past a vertical barrier of height b in a uniformly stratified ocean of depth $h > b$ and buoyancy frequency N. The radiated power (watts per metre of barrier) is

$$\tfrac{1}{4}\pi\rho_0 b^2 U^2 N \sqrt{1 - (f/\omega)^2} M(b/h),$$

where ρ_0 is the mean density of seawater, $U\cos(\omega t)$ the tidal velocity, and f the Coriolis frequency. The function $M(b/h)$ increases monotonically with $M(0) = 1$, $M(0.92) = 2$ and $M(1) = \infty$. As $b/h \to 1$, M diverges logarithmically and consequently the radiated power grows as $\ln[(h - b)/b]$. We also calculate the conversion in a realistically stratified ocean with strongly non-uniform buoyancy frequency, $N(z)$. A rough approximation to the radiated power in this case is

$$\tfrac{1}{4}\pi\rho_0 b^2 U^2 N(b)\sqrt{1 - (f/\omega)^2} M(B/\pi),$$

where $N(b)$ is the buoyancy frequency at the tip of the ridge and B is the height of the ridge in WKB coordinates. (The WKB coordinate is normalized so that the total depth of the ocean is π.) The approximation above is an over-estimate of the actual radiation by as much as 20% when $B/\pi \approx 0.8$. But the formula correctly indicates the strong dependence of conversion on stratification through the factor $N(b)$.

1. Introduction

In the deep ocean, tidal velocities of 1 or $2\,\text{cm}\,\text{s}^{-1}$ are more rapid than most other abyssal flows. The interaction of these tides with submarine topography results in the radiation of internal gravity waves into the interior. These disturbances, known as the 'internal tide' (Wunsch 1975), are a source of the energy required to overturn and mix the stably stratified abyss (Munk & Wunsch 1998; Ledwell *et al.* 2000).

The main theoretical approach to estimating the rate of tidal conversion (expressed in watts of radiated power) has been the weak topography approximation (WTA), developed first by Bell (1975*a*, *b*). Bell assumes that the buoyancy frequency is uniform and that the ocean is vertically unbounded. These two restrictions are not essential to Bell's approach: instead the crucial ingredients in the WTA are the assumptions that topographic slopes are small and that the height of the topography is much less than the depth of the ocean. In this case the bottom boundary condition can be applied approximately at a flat surface, say $z = 0$, rather than at the actual bumpy bottom. This simplification allows the linear superposition of different topographic sinusoids. In other words, Fourier analysis is applicable and the conversion rate is obtained
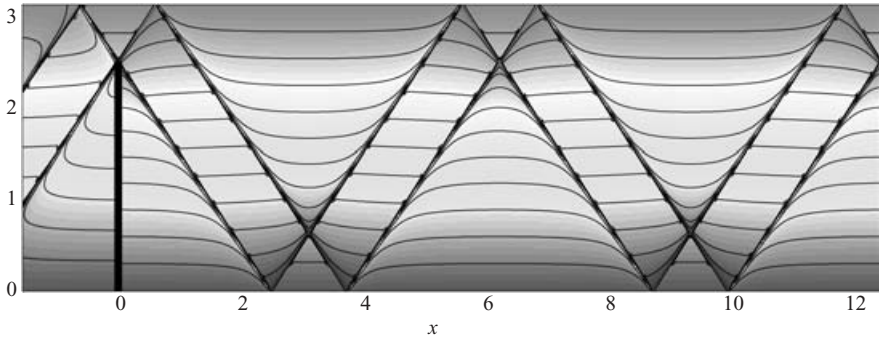
FIGURE 1. The idealized ridge is the heavy vertical line segment at $x = 0$; the ridge height is $b/h = 0.8$. This illustration uses the analytic solution in (4.17) with an unrealistically large value $\alpha = 0.1$ in order to clearly display the distortion of the isopycnal surfaces.

in terms of the topographic spectral density. St. Laurent & Garrett (2002) used this approach to estimate the tidal conversion occurring at the East Pacific Rise and at the mid-Atlantic Ridge. Llewellyn Smith & Young (2002) made a similar estimate of the tidal conversions produced by the global inventory of 1.4 million seamounts. In both of these applications, simple estimates indicate that the WTA is likely to be valid. Indeed, the results of Balmforth, Ierley & Young (2002) encourage the view that the WTA is accurate over the whole subcritical range in which the ray slope is less (but not much less) than the topographic slopes.

Subsequent developments of the WTA have included finite depth effects and non-uniform buoyancy frequency (Llewellyn Smith & Young 2002; Khatiwala 2003). Analytic (Baines 1973, 1982; Balmforth *et al.* 2002) and numerical (Holloway & Merrifield 1999; Li 2003; Khatiwala 2003) studies have lifted the weak-topography restriction. Nevertheless published analytic results are limited to the subcritical regime in which the topographic slope is less than the ray slope of the internal tide.

St. Laurent *et al.* (2003) have taken a fresh approach by considering very steep submarine topography, idealized as a 'knife-edge' obstruction. Tidal conversion by a knife-edge is a two-dimensional, (x, z), problem in which the ocean surface is at $z = h$, while the bottom is the set

$$\mathscr{B} \equiv \{x = 0, 0 < z < b\} \bigcup \{-\infty < x < \infty, z = 0\}. \tag{1.1}$$

Since $h > b$ the gap above the crest of this idealized ridge has height $h - b$ (see figure 1). This knife-edge profile is the antithesis of the gently sloping topographies considered by the WTA. Thus, although this is a considerable idealization, a close examination of the knife-edge ridge is perhaps the best hope for understanding tidal conversion at strongly supercritical topography.

The knife-edge geometry has been previously examined in the context of internal wave scattering (rather than generation) by Larsen (1969) and by Robinson (1969). Our results in this paper rely heavily on Robinson's formulation. Robinson obtained an analytic expression for the Green's function, or 'vortex solution', of the internal gravity wave equation with uniform buoyancy frequency, N. We extend Robinson's results slightly by using the WKB approximation to obtain the Green's function with non-uniform buoyancy frequency, $N(z)$. This Green's function represents waves propagating away from a point source in an ocean of finite depth h and with realistically non-uniform $N(z)$. By superposing these singular solutions with a weight

function one can represent the effects of the knife-edge ridge and so transform either scattering or generation problems into an integral equation. The solution of this integral equation is the weight function. In the case of uniform stratification the integral equation can be transformed into a well-known form, familiar from aerofoil theory, and thus solved exactly. All of this was done by Robinson (1969) for the scattering problem, and in this work we have adapted Robinson's results to the generation problem. With these techniques we can go beyond the numerical approach of St. Laurent *et al.* (2003) by obtaining analytic expressions for the conversion rate at all values of the non-dimensional parameter b/h. Additionally, by numerically solving the integral equation, we can treat realistically non-uniform buoyancy frequency which varies by a factor of fifty between the abyss and the thermocline.

2. Formulation

2.1. *Governing equations*

We idealize the ocean as a rotating, inviscid fluid layer in which the tide sloshes to-and-fro in the x-direction; z denotes the vertical. The barotropic tide is modelled as the periodically reversing, spatially uniform flow:

$$\boldsymbol{U} = U\cos(\omega t)\hat{\boldsymbol{x}}. \tag{2.1}$$

Conversion to internal gravity waves occurs because this tide flows over the knife-edge ridge. The density is written as

$$\rho = \rho_0\left[1 - g^{-1}\int_0^z N^2(z')\,\mathrm{d}z' - g^{-1}b\right], \tag{2.2}$$

where ρ_0 is the mean density of seawater, $N(z)$ is the buoyancy frequency and $b(x, z, t)$ is the disturbance. Because the topography is independent of y, so too is the disturbance created by tidal action. The governing equations for the induced velocity (u, v, w), rescaled pressure p and buoyancy b, are

$$\left.\begin{array}{ll} u_t - fv + p_x = 0, & v_t + fu = 0, \\ p_z = b, \quad b_t + N^2 w = 0, & u_x + w_z = 0. \end{array}\right\} \tag{2.3}$$

In these equations f is the Coriolis frequency.

The velocity in the (x, z)-plane can be represented using a streamfunction $\psi(x, z, t)$: $(u, w) = (-\psi_z, \psi_x)$. The problem then reduces to solving the internal gravity wave equation,

$$\psi_{zztt} + f^2\psi_{zz} + N^2\psi_{xx} = 0. \tag{2.4}$$

The bottom boundary condition is

$$\psi(\boldsymbol{x} \in \mathscr{B}) = Uz\cos(\omega t), \tag{2.5}$$

where $\mathscr{B}$ is the set in (1.1). The condition in (2.5) ensures that the total streamfunction, $-Uz\cos(\omega t) + \psi$, vanishes on $\mathscr{B}$.

Replacing a ridge of thickness $\sim 100\,\mathrm{km}$ by a knife-edge barrier is a considerable idealization. However this simplification is probably justified provided that the slope of the ridge is much greater than the slope of the internal tidal beams. Equivalently, one requires that the beams generated at the top of the ridge reflect from the ocean floor, rather than the flanks of the ridge. Rough numerical estimates indicate that the Hawaiian Ridge satisfies these conditions. As an illustration, see figure 8 of
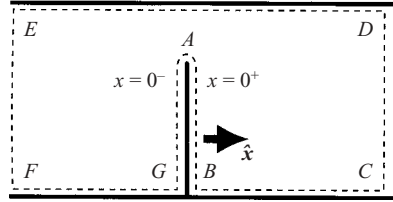
FIGURE 2. The energy flux J enters the control volume $ABCDEFG$ through the ridge GAB. The energy leaves through EF and DC. The conversion $\mathscr{C}$ in (2.12) is obtained by integrating $J \cdot \hat{x}$ along the segment AB, and multiplying by 2 to account for the flux through GA.

Merrifield & Holloway (2002), which shows a simulation of Hawaiian tidal conversion: the emitted internal disturbances do not subsequently interact with the flanks of the ridge.

The hydrostatic approximation is valid provided that $\omega/N \ll 1$ and linearization is valid provided that the tidal excursion (about 100 m) is much less than the width of the topography. For further discussion of linearization see Robinson (1969), Balmforth *et al.* (2002), St. Laurent & Garrett (2002), Llewellyn Smith & Young (2002), and §4.3.

2.2. *The steady-state wave field*

We consider the steady-state wave conversion by looking for time-periodic solutions with the tidal frequency: we introduce $\varphi = \varphi_r + i\varphi_i$, where

$$\psi = U\mathrm{Re}\{e^{-i\omega t}\varphi\} = U(\varphi_r \cos \omega t + \varphi_i \sin \omega t). \qquad (2.6)$$

The function φ satisfies the hyperbolic equation

$$N^2\varphi_{xx} = (\omega^2 - f^2)\varphi_{zz}, \qquad \varphi(x \in \mathscr{B}) = z, \qquad \varphi(x, h) = 0. \qquad (2.7)$$

The mathematical problem is completed by insisting that the energy flux is away from the knife. This radiation condition ensures that φ has both a real and an imaginary part.

2.3. *Energy flux and conversion*

The main quantity of interest is the conversion rate of barotropic tidal energy into internal gravity waves. To calculate the conversion rate we begin with the energy equation obtained from (2.3):

$$\tfrac{1}{2}(u^2 + v^2 + N^{-2}b^2)_t + \psi_x p_z - \psi_z p_x = 0. \qquad (2.8)$$

For the periodic flow, the average of (2.8) over the tidal cycle implies that

$$\nabla \cdot J = 0, \qquad (2.9)$$

where J is the phase-average of the energy flux $(\psi p_z, -\psi p_x)$; using (2.6) this phase-averaged flux can be written as

$$J = \frac{iU^2\rho_0}{4\omega}[N^2(\varphi\varphi_x^* - \varphi^*\varphi_x), -(\omega^2 - f^2)(\varphi\varphi_z^* - \varphi^*\varphi_z)]. \qquad (2.10)$$

The easiest way to calculate the conversion is to observe that on the segment AB in figure 2, where $x = 0^+$ and $\varphi = \varphi^* = z$, the flux of energy into the fluid is

$$J \cdot \hat{x} = \frac{U^2\rho_0}{2\omega}N^2 z\varphi_{ix}(0^+, z). \qquad (2.11)$$

We are considering $x = 0^+$ so on the left-hand side of (2.11) $\hat{x}$ is the inward normal. The total conversion is then

$$\mathscr{C} = \frac{U^2 \rho_0}{\omega} \int_0^b N^2(z) z \varphi_{ix}(0^+, z)\, \mathrm{d}z. \tag{2.12}$$

There is a factor of 2 included in (2.12) to account for the flux of energy through $x = 0^-$. To summarize: all that is needed to calculate the conversion is the normal derivative $\varphi_{ix}(0^\pm, z)$.

3. The Green's function and the integral equation

We solve (2.7) using the Green's function method developed by Robinson (1969) to study scattering of internal gravity waves from a knife-edge barrier. The biographical article by Fowkes & Silberstein (1995) has some interesting comments on the history of this problem and the confusion surrounding the radiation condition.

3.1. *Vertical normal modes and WKB*

We use the vertical normal modes of the stratification $N(z)$ which are defined by the eigenproblem

$$\frac{\mathrm{d}^2 a_n}{\mathrm{d}z^2} + c_n^{-2} N^2 a_n = 0, \qquad a_n(0) = a_n(h) = 0. \tag{3.1}$$

The eigenvalue c_n is the phase speed of mode n and $\lambda_n \equiv c_n/f$ is the radius of deformation. We take a_n to be dimensionless. The orthogonality condition is

$$\int_0^h a_n(z) a_m(z) N^2(z)\, \mathrm{d}z = \varpi_n \delta_{mn}, \tag{3.2}$$

where ϖ_n is the normalization constant of mode n.

We develop the WKB approximation by first introducing the vertically averaged buoyancy frequency and the non-dimensional buoyancy frequency:

$$\bar{N} \equiv \frac{1}{h} \int_0^h N(z')\, \mathrm{d}z', \quad \mathcal{N}(z) \equiv N(z)/\bar{N}. \tag{3.3}$$

The WKB stretched coordinate is

$$Z \equiv \frac{\pi}{h} \int_0^z \mathcal{N}(z')\, \mathrm{d}z', \tag{3.4}$$

where $0 < Z < \pi$. With this notation the WKB approximation to the eigenfunctions is

$$a_n(z) \approx \frac{\sin(nZ)}{\sqrt{\mathcal{N}}}. \tag{3.5}$$

We also find that $c_n \approx h\bar{N}/n\pi$ and $\varpi_n \approx \frac{1}{2} \bar{N}^2 h$.

3.2. *The Green's function*

The main tool used in this work is the Green's function $\mathscr{G}(x, z, z')$ defined by

$$N^2 \mathscr{G}_{xx} - (\omega^2 - f^2) \mathscr{G}_{zz} = \mathscr{G}_0 \delta(x) \delta(z - z'), \tag{3.6}$$

with the boundary conditions

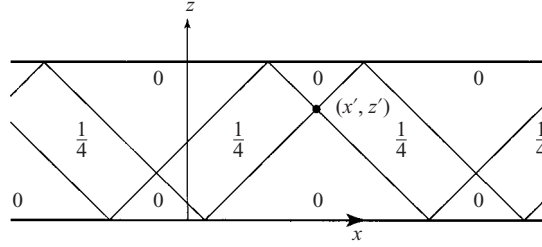$$\mathscr{G}(x, 0, z') = \mathscr{G}(x, h, z') = 0. \tag{3.7}$$

FIGURE 3. The imaginary part of $\mathscr{G}_{\mathrm{WKB}}(x - x', z, z')$ in (3.13). The source is at (x', z') and the stratification is uniform ($\mathscr{N} = \mathscr{N}' = 1$). This figure corrects an inconsequential (but confusing) error in Robinson's figure 1.

The definition of $\mathscr{G}$ is completed by requiring that there is only outgoing radiation. We will choose the normalization constant $\mathscr{G}_0$ in (3.6) later.

Using the vertical normal modes, this Green's function is

$$\mathscr{G}(x, z, z') = \mathscr{G}_0 \sum_{n=1}^{\infty} \frac{\mathrm{e}^{\mathrm{i}\kappa_n|x|}}{2\mathrm{i}\kappa_n \varpi_n} a_n(z) a_n(z'), \tag{3.8}$$

with

$$\kappa_n \equiv \frac{\sqrt{\omega^2 - f^2}}{c_n}. \tag{3.9}$$

The $|x|$ in the exponential on the right-hand side of (3.8) ensures that radiation is outgoing on both sides of the source at $x = 0$.

Using the WKB approximation we find that $\kappa_n \approx n\pi/\mu h$ where

$$\mu \equiv \frac{\bar{N}}{\sqrt{\omega^2 - f^2}}. \tag{3.10}$$

We also define $X \equiv \pi x/\mu h$ and choose the normalization $\mathscr{G}_0 = \mathrm{i}\bar{N}^2/\mu$. Thus the WKB Green's function is

$$\mathscr{G}_{\mathrm{WKB}}(x, z, z') = \sum_{n=1}^{\infty} \frac{\sin nZ \sin nZ'}{n\pi \sqrt{\mathscr{N}(z)\mathscr{N}(z')}} \mathrm{e}^{\mathrm{i}n|X|}. \tag{3.11}$$

In (3.11) $Z(z)$ is the WKB coordinate defined in (3.4). This expression agrees with that of Robinson (1969) in the limit of uniform stratification ($\mathscr{N}(z) = \mathscr{N}(z') = 1$ and $Z = \pi z/h$).

Following Robinson, the series in (3.11) can be summed exactly and expressed concisely using the function

$$\bowtie(X, Z, Z') \equiv \frac{\sin\left(\frac{1}{2}(|X| + Z + Z')\right) \sin\left(\frac{1}{2}(|X| - Z - Z')\right)}{\sin\left(\frac{1}{2}(|X| + Z - Z')\right) \sin\left(\frac{1}{2}(|X| - Z + Z')\right)}. \tag{3.12}$$

The result is

$$\mathscr{G}_{\mathrm{WKB}}(x, z, z') = \frac{1}{4\pi} \frac{1}{\sqrt{\mathscr{N}\mathscr{N}'}} [\ln |\bowtie| + \mathrm{i}\pi H(-\bowtie)], \tag{3.13}$$

where $\mathscr{N}' \equiv \mathscr{N}(z')$. Figure 3 shows the imaginary part of $\mathscr{G}_{\mathrm{WKB}}(x - x', z, z')$.

3.3. *The integral equation*

Using $\mathcal{G}_{WKB}(X, Z, Z')$ we represent the solution of (2.7) as

$$\varphi(x, z) = \int_0^b \gamma(z') \mathcal{G}_{WKB}(x, z, z') \, dz'. \tag{3.14}$$

On the knife, $x = 0$, $\varphi = z$ and $\mathcal{G}_{WKB}$ also simplifies. Thus (3.14) collapses to an integral equation for the source density γ:

$$\sqrt{\mathcal{N}(z)} z = \frac{1}{2\pi} \int_0^b \frac{\gamma(z')}{\sqrt{\mathcal{N}(z')}} \ln \left| \frac{\sin\left(\frac{1}{2}(Z + Z')\right)}{\sin\left(\frac{1}{2}(Z - Z')\right)} \right| dz'. \tag{3.15}$$

One can show from (3.14) that

$$\varphi_{ix}(0^{\pm}, z) = \pm \frac{\gamma(z)}{2\mu \mathcal{N}^2}, \tag{3.16}$$

so that from (2.12) the conversion is given by

$$\mathcal{C} = \tfrac{1}{2} \rho_0 U^2 \sqrt{1 - \frac{f^2}{\omega^2}} \bar{N} \int_0^b z \gamma(z) \, dz. \tag{3.17}$$

Thus the problem devolves to solving (3.15) for $\gamma(z)$ and computing the integral in (3.17).

4. Uniform stratification

In this section we consider the special case of a uniform stratification so that $\mathcal{N} = 1$ and $Z = \pi z / h$. Using the non-dimensional vertical coordinate Z, the integral equation (3.15) becomes

$$Z = \frac{1}{2\pi} \int_0^B \Gamma(Z') \ln \left| \frac{\sin\left(\frac{1}{2}(Z + Z')\right)}{\sin\left(\frac{1}{2}(Z - Z')\right)} \right| dZ', \tag{4.1}$$

where $B \equiv \pi b / h$ and $\Gamma(Z') \equiv \gamma(z')$. Taking the derivative of (4.1) with respect to Z we have

$$2 = \int_0^B \frac{\Gamma(Z') \sin Z'}{\cos Z - \cos Z'} \frac{dZ'}{\pi}. \tag{4.2}$$

Changing variables in (4.2) to

$$\nu \equiv 2 \frac{1 - \cos Z}{1 - \cos B} - 1, \tag{4.3}$$

and defining $\Upsilon(\nu') = \Gamma(Z')$, produces a standard form:

$$-2 = \int_{-1}^1 \frac{\Upsilon(\nu')}{\nu - \nu'} \frac{d\nu'}{\pi}. \tag{4.4}$$

This is a special case of the airfoil equation – a Cauchy singular integral equation of the first kind. The general solution of (4.4) (e.g. see Tuck 1980 or Carrier, Krook & Pearson 1983) is $\Upsilon(\nu) = (\Lambda + 2\nu)/\sqrt{1 - \nu^2}$ where Λ is a 'constant of integration'. To determine Λ we argue that $\Gamma(Z)$ must be non-singular at $Z = 0$. This regularity

condition implies that $\Upsilon(\nu)$ must be non-singular at $\nu = -1$ so that $\Lambda = 2$. Thus the solution of (4.1) is

$$\Upsilon(\nu) = 2\sqrt{\frac{1+\nu}{1-\nu}}, \quad \Gamma(Z) = 2\sqrt{\frac{1-\cos Z}{\cos Z - \cos B}}. \tag{4.5}$$

4.1. *The conversion*

With $\Gamma(z)$ to hand, the conversion can now be computed using (3.17):

$$\mathscr{C} = \rho_0 U^2 N \sqrt{1 - \frac{f^2}{\omega^2}} \frac{h^2}{\pi^2} K(B/\pi), \tag{4.6}$$

where

$$K(B/\pi) \equiv \int_0^B Z \sqrt{\frac{1-\cos Z}{\cos Z - \cos B}} \, dZ. \tag{4.7}$$

For numerical and asymptotic evaluation of the integral it is convenient to use the variable

$$\tau \equiv \tan(B/2) = \tan(\pi b/2h). \tag{4.8}$$

Making this change of variables puts the integral (4.7) in the form

$$K(B/\pi) = 4\sqrt{1+\tau^2} \int_0^\tau \frac{t \tan^{-1} t}{\sqrt{\tau^2 - t^2}} \frac{dt}{1+t^2}, \tag{4.9}$$

and then asymptotic methods give the approximations:

$$K(B/\pi) \approx \begin{cases} \pi\tau^2/\sqrt{1+\tau^2} & \text{if } \tau \ll 1 \\ 2\pi\sqrt{1+\tau^2} \ln \tau/\tau & \text{if } \tau \gg 1. \end{cases} \tag{4.10}$$

Further reductions of the small-τ approximation in (4.10) give the conversion rate for a knife-edge immersed in an ocean of infinite depth as

$$\mathscr{C} \approx \tfrac{1}{4}\pi b^2 \rho_0 U^2 N \sqrt{1 - \frac{f^2}{\omega^2}}. \tag{4.11}$$

Equation (4.11) confirms the numerical speculation of St. Laurent *et al.* (2003) that in the limit $h \to \infty$ the conversion due to a knife-edge ridge is precisely twice that of Bell's (1975a) witch with the same height, b. With $f = 0$, (4.11) is also a special case of Hurley's (1997) formula for the energy radiated by a vibrating ellipse in an unbounded stratified fluid. Note that the knife-edge radiates energy into the whole upper half-plane and hence its power output is twice the single-quadrant result of Hurley.

It is convenient to use the small-b/h limit in (4.11) to rewrite the conversion in (4.6) as

$$\mathscr{C} = \tfrac{1}{4}\pi b^2 \rho_0 U^2 N \sqrt{1 - \frac{f^2}{\omega^2}} M(B/\pi), \tag{4.12}$$

where
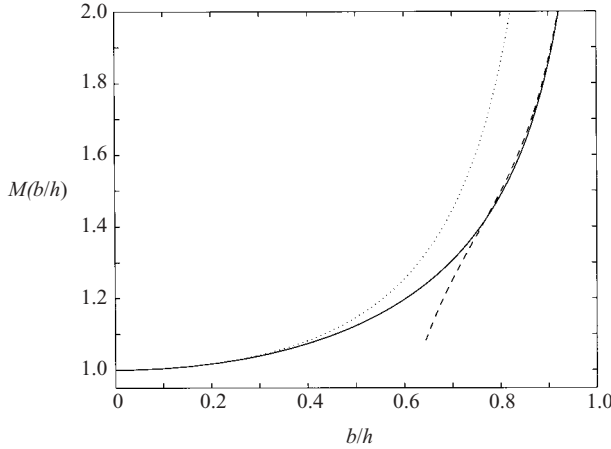
$$M(B/\pi) \equiv \frac{4K(B/\pi)}{\pi B^2}. \tag{4.13}$$

FIGURE 4. The solid curve is M defined by (4.7) and (4.13), as a function of $b/h = B/\pi$; $M(b/h)$ appears in (4.12) as the 'enhancement factor' by which $\mathscr{C}$ exceeds the $b/h \ll 1$ limit in (4.11). St. Laurent *et al.* (2003) obtain a similar curve using a different method. The dotted and dashed curves are the approximations based on (4.10).

The function $M(B/\pi)$, along with approximations based on (4.10), is shown in figure 4. Although $M \to \infty$ as $b/h = B/\pi \to 1$, the initial rise of M is not so dramatic; e.g. it is not until $b/h \approx 0.92$ that $M = 2$.

4.2. *Projection onto the vertical modes*

Now we turn to the modal projection. Substituting (3.11) (with $\mathscr{N}(z) = \mathscr{N}(z') = 1$) into the representation (3.14) gives

$$\varphi(X, Z) = \frac{h}{\pi} \sum_{n=1}^{\infty} n^{-1} PP_n \sin nZ \, e^{in|X|}. \tag{4.14}$$

In (4.14)

$$PP_n \equiv P_{n-1}(\cos B) - P_n(\cos B), \tag{4.15}$$

where P_n is the nth Legendre polynomial. The key result used to obtain (4.14) is

$$\frac{2}{\pi} \int_0^B \sin nZ \sqrt{\frac{1 - \cos Z}{\cos Z - \cos B}} \, dZ = P_{n-1}(\cos B) - P_n(\cos B). \tag{4.16}$$

To visualize the solution we use the total buoyancy field, $b_* \equiv N^2 z + b(x, z, t)$, obtained from (4.14)†. After some working we find

$$b_*(x, z, t) = \frac{N^2 h}{\pi} \left[Z + \alpha \mathrm{Re} \left(e^{-i\omega t} \sum_{n=1}^{\infty} PP_n \sin nZ \, \mathrm{sgn}(X) e^{in|X|} \right) \right], \tag{4.17}$$

where

$$\alpha \equiv \frac{\pi U}{Nh} \sqrt{1 - \frac{f^2}{\omega^2}}. \tag{4.18}$$

† Notice that b denotes both the buoyancy perturbation – as in (2.2) – and the height of the ridge. The context will clearly indicate which is which.
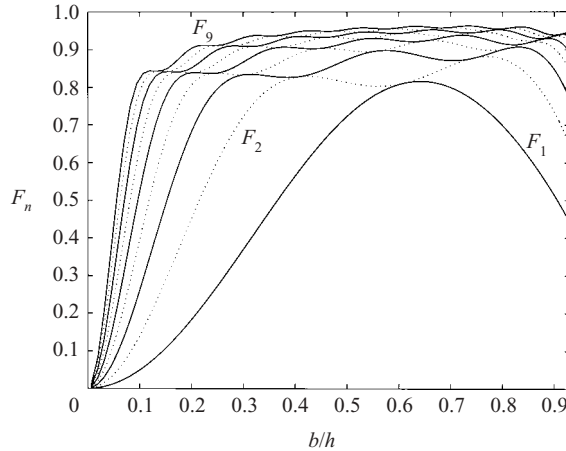
FIGURE 5. Fraction of the converted energy in the first n modes with $n = 1, 2, \ldots, 9$ as a function of $b/h = B/\pi$. The even values F_2 to F_8 are shown as dotted curves. The function $F_n(B/\pi)$ is defined in (4.21).

Figure 1 shows the solution (4.17) at $t = 0$ with $\alpha = 0.1$. In this illustration the sum was truncated at $n = 200$ and the series was further filtered to remove Gibbs oscillations which would otherwise be prominent in the tidal beams emanating from the ridge crest.

We can also use the series in (4.14) to calculate the modal conversion via

$$\mathcal{C} = 2 \int_0^h \boldsymbol{J}(x > 0, z) \cdot \hat{\boldsymbol{x}} \, \mathrm{d}z \tag{4.19}$$

where $\boldsymbol{J}$ is the flux in (2.10) and the factor of 2 on the right-hand side accounts for the energy radiated to $x < 0$. This approach, which amounts to computing the flux of energy through EF and CD in figure 2, provides the following alternative expression for the integral K defined in (4.7):

$$K(B/\pi) = \frac{\pi}{2} \sum_{n=1}^{\infty} n^{-1} PP_n^2. \tag{4.20}$$

From (4.20) we can obtain the fraction of the converted energy contained in the first n modes:

$$F_n(B/\pi) = \sum_{k=1}^{n} k^{-1} PP_k^2 \bigg/ \sum_{k=1}^{\infty} k^{-1} PP_k^2. \tag{4.21}$$

Figure 5 shows $F_1(B/\pi)$ to $F_9(B/\pi)$. At about $\tau = 1.4$ the curve F_2 kisses F_1 which indicates that there is no energy in mode 2 for a ridge with $b/h \approx 0.6$. In general F_n kisses F_{n+1} at n points.

St. Laurent *et al.* (2003) present a numerical result for the fraction of energy in mode 1, F_1. These authors note that at $b/h = 0.75$ mode 1 carries 75% of the total flux, and 75% is close to the fraction observed at Hawaii (Egbert & Ray 2000, 2001; Ray & Mitchum 1996).

4.3. *The validity of linearization and tidal beams*

With the reconstructed solution in (4.17) we can make an *a posteriori* assessment of the linearization approximation. In order that the displacement of the isopycnals be

small, we certainly require that $\alpha \equiv \pi U \sqrt{1 - (f/\omega)^2}/(Nh)$ be much less than one. A rough numerical estimate taking $U = 0.01\,\mathrm{m\,s^{-1}}$, $N = 1$ cycles per hour (c.p.h.), and $h = 5000\,\mathrm{m}$ shows that α is less than 0.004. (In figure 1 we use the unrealistically large value $\alpha = 0.1$ to make the isopycnal displacements visible.)

The condition $\alpha \ll 1$ ensures that linearization is valid over most of the domain. But $\alpha \ll 1$ does not ensure that displacements are small within the singular beams which originate from the top of the barrier in figure 1. Robinson (1969) remarks that the buoyancy perturbation diverges like $|\xi|^{-1/2}$, where ξ is the normal distance from the beam. In other words, the perturbation density becomes infinite within the beams. This singularity indicates a failure of linear non-dissipative theory, albeit in a small part of the domain.

The singularity is not an artefact of the knife-edge geometry: Balmforth *et al.* (2002) document the formation of singular tidal beams by a smooth topographic sinusoid with critical slope. That is, the singularity is a consequence of supercritical slope rather than the knife-edge. Just as in the much-studied problem of internal wave reflection by a sloping boundary, the singularity indicates that mixing and mode conversion might occur.

Our main focus is the energy conversion and it is our hope that the results such as (4.6) are reliable even though linear theory fails in part of the domain. One supportive argument is the analysis of Robinson (1969) which shows that the beam singularity is not a source of mass, momentum or energy. A second point is that Balmforth *et al.* (2002) have computed the conversion produced by a topographic sinusoid as a function of the amplitude of the sinusoid. The conversion increases with topographic amplitude until the topographic slope becomes critical, and the wave-field singular. Nevertheless there is no evidence of this singularity in the conversion rate, which is always a smooth function of the topographic amplitude.

5. Non-uniform stratification

A more realistic model is obtained by taking the buoyancy frequency to be non-uniform. The integral equation (3.15) can be rewritten using Z in (3.4) as the vertical coordinate. In this form (3.15) becomes

$$L(Z) = \frac{1}{2\pi} \int_0^B \Gamma(Z') \ln \left| \frac{\sin\left(\frac{1}{2}(Z + Z')\right)}{\sin\left(\frac{1}{2}(Z - Z')\right)} \right| \mathrm{d}Z', \tag{5.1}$$

where now

$$B \equiv \frac{\pi}{h} \int_0^b \mathcal{N}(z')\,\mathrm{d}z' \tag{5.2}$$

is the ridge height in terms of the WKB coordinate. Also in (5.1),

$$\Gamma(Z) \equiv \gamma(z)/\mathcal{N}^{3/2}(z), \qquad L(Z) \equiv \frac{\pi z}{h}\sqrt{\mathcal{N}}. \tag{5.3}$$

Once we have solved (5.1) for $\Gamma(Z)$ the conversion is obtained from (3.17) as

$$\mathscr{C} = \rho_0 U^2 \bar{N} \sqrt{1 - \frac{f^2}{\omega^2}} \frac{h^2}{\pi^2} K(B/\pi), \tag{5.4}$$

where now

$$K(B/\pi) = \frac{1}{2} \int_0^B L(Z)\Gamma(Z)\,\mathrm{d}Z. \tag{5.5}$$

(Notice that the WKB coordinate is normalized so that $Z = \pi$ is the ocean surface; we anticipate that $K(B/\pi) \to \infty$ as $B/\pi \to 1$.)

The integral equation (5.1) was solved numerically by discretizing the WKB coordinate, Z, and using the method reviewed by Tuck (1980). Both midpoint and trapezoidal discretizations of the integral gave the same answer to four significant figures. The accuracy of the conversion rate was also checked by solving the constant-N case numerically and comparing the result to the exact solution in (4.5). With 200 gridpoints the conversion obtained numerically from (5.5) agreed with (4.7) to three significant figures.

5.1. *A model stratification*

We choose a simple model for the buoyancy frequency, consisting of an exponentially varying portion and a constant term. The form of N is then

$$N = N_B + N_C\left(e^{z/d} - 1\right). \tag{5.6}$$

The average buoyancy frequency and the WKB coordinate introduced in (3.4) are

$$\bar{N} = N_B + N_C\left[\frac{e^{\beta} - 1}{\beta} - 1\right], \tag{5.7}$$

where $\beta \equiv h/d$, and

$$Z = \pi\frac{z + (N_C/N_B)\left(de^{z/d} - d - z\right)}{h + (N_C/N_B)(de^{\beta} - d - h)} \tag{5.8}$$

respectively. The relation (5.8) cannot be inverted for z as a function of Z and consequently $L(Z)$ in (5.3) must be computed numerically on the grid points. The integral K in (5.5) is a function of b/h, β and ϖ, where $\varpi \equiv \bar{N}/N_B$ is the ratio of the average buoyancy frequency to the buoyancy frequency at the bottom. Thus, using the model stratification in (5.6), the conversion is

$$\mathscr{C} = \rho_0 U^2 \bar{N}\sqrt{1 - \frac{f^2}{\omega^2}}\frac{h^2}{\pi^2}K(b/h, \beta, \varpi). \tag{5.9}$$

Notice that the model stratification becomes uniform if either $\beta = 0$ or $\varpi = 1$; in these two cases $K(b/h, \beta, \varpi)$ in (5.9) reduces to $K(b/h)$ in (4.6) and (4.7). Thus we recover as a special case the conversion with uniform stratification.

We estimated the parameters N_B, N_C and d in (5.6) using the World Ocean Database 2001 (Conkright *et al.* 2001). All the casts in the WOD reaching below 5000 m within a $20° \times 20°$ square centred on Hawaii were assembled; there are 94 such density profiles. Temperature and salinity were interpolated at 2 m intervals between 50 m and 5000 m and the buoyancy frequency was computed for each of the 94 casts. A relatively smooth N^2-profile was produced by averaging the 94 casts. We defined a penalty function by integrating the square of the difference between the data N^2 and the model N^2 in (5.6) over the range of depths 500 m to 5000 m. This integral was also weighted using the error in the mean. The three parameters N_B, N_C and $\beta = h/d$ were then found using a nonlinear optimization procedure to minimize the penalty function. The resulting values of the model parameters are given in the second row of table 1.

To make a second comparison, we used station ALOHA at 22°45.0′N, 158°00.0′W from the Hawaii Ocean Time Series (HOTS 2002). A single cast from cruise 111 of HOTS between 1 February and 4 February 2000 was chosen. The values from the nonlinear fitting procedure described above are shown in third row of table 1. (The

Data	h (m)	N_B (c.p.h.)	N_C (c.p.h.)	β	$\bar{N}$ (c.p.h.)	c_1 (m s^{-1})	b (m)	K	$\mathscr{C}$ (GW)
Constant N	5000	–	–	–	1.00	2.78	4500	11.7	9.6
WOD	5000	0.35	0.0115	5.85	1.02	2.68	4500	19.7	16.6
HOTS	4806	0.50	0.0010	8.74	1.22	2.99	4325	17.9	16.6

TABLE 1. Parameter values for the constant-N model, WOD data and HOTS ALOHA data. We estimate the conversion by assuming the ridge to be 2000 km long; $U = 0.01$ m s^{-1}, $f = 5 \times 10^{-5}$ s^{-1}, $\omega = 2.8 \times f$ and $\rho_0 = 1000$ kg m^{-3}. The seventh column gives c_1, the phase speed of the first baroclinic mode obtained by solving the eigenproblem (3.1). As an assessment of the WKB approximation we note the the WKB estimate, $c_1 \approx h\bar{N}/\pi$, has an error of 2% for WOD and 8% for HOTS.

fitting no longer weights the integrand since with a single profile there is no estimate of the error in N^2.)

The data and model N^2 profiles are shown in figure 6(a). The fit is satisfactory below 500 m. Trying to fit above 500 m is difficult because of contamination by the seasonal cycle and mixed-layer effects. Shown in figure 6(b) is the integral K as a function of b/h using the stratification parameters in rows 2 and 3 of table 1: K increases steeply over the range $0.75 < b/h < 0.95$ so that the conversion increases by a factor of 10 if b/h increases from 0.75 to 0.95.

Figure 6(c) shows K as a function of β and $\varpi \equiv \bar{N}/N_B$, for a fixed value of $b/h = 0.9$. These two parameters are sufficient to characterize the model profile in (5.6) if $\bar{N}$ is also known. The locations of the WOD and HOTS data are shown by $\times$ and $+$ respectively.

Figure 7 shows the fraction of converted energy in the first 9 modes for the HOTS buoyancy profile over a range of ridge heights. Figure 7(a) has b/h as the abscissa while figure 7(b) has B/π. Using B/π in figure 7(b) ensures that the structure of the F_n is very similar to that of figure 5.

5.2. Sensitivity of conversion rate to the buoyancy frequency

The preceding results show that as b/h increases the conversion rate $\mathscr{C}$ rises rapidly, e.g. figure 6(b). This rapid increase occurs because the ridge penetrates the heavily stratified upper ocean, and tidal conversion is more efficient if N is large. To quantify this important property of non-uniform stratification we develop an approximate solution of the integral equation (5.1) which makes the dependence of $\mathscr{C}$ on the parameters of the model stratification transparent.

The idea is to approximate the left-hand side of (5.1) by

$$L(Z) \approx \frac{ZL(B)}{B} \tag{5.10}$$

(see figure 8a) so that our earlier solution of (4.1) gives

$$\Gamma(Z) \approx 2\frac{L(B)}{B}\sqrt{\frac{1 - \cos Z}{\cos Z - \cos B}}. \tag{5.11}$$

Substituting the approximations (5.10) and (5.11) into (5.4) and (5.5), we eventually find that the conversion is

$$\mathscr{C} \approx \frac{\pi}{4}\rho_0 U^2 \sqrt{1 - \frac{f^2}{\omega^2}} N(b)b^2 M(B/\pi). \tag{5.12}$$
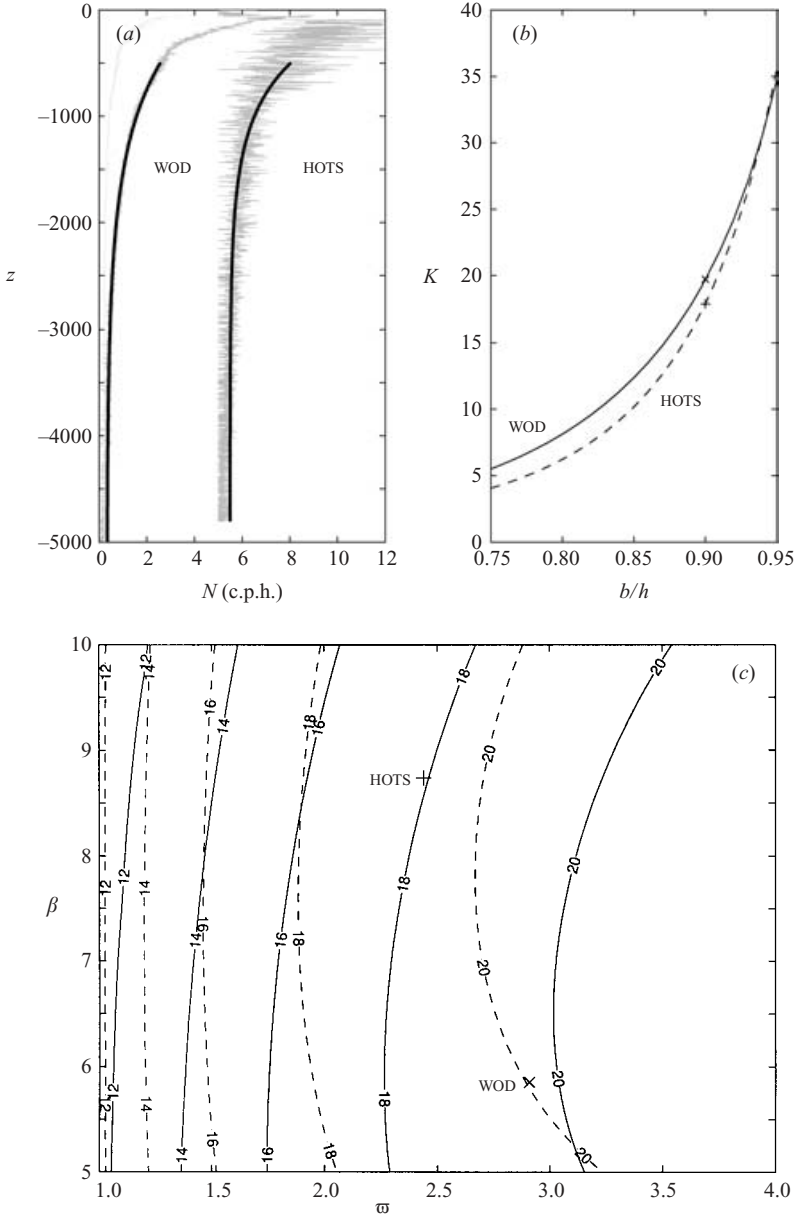
FIGURE 6. (*a*) Observed $N^2(z)$ profiles: grey lines are N^2 means (and standard deviations for WOD – this is the curve with smaller variations); bold line is the model in (5.6) using the parameters in table 1. The HOTS profile is offset by 5 c.p.h. (*b*) K as a function of b/h using the stratification parameters in the second and third rows of table 1. (*c*) The solid curves show K as a function of $\beta \equiv h/d$ and $\varpi \equiv \bar{N}/N_B$, with $b/h = 0.9$. The dashed curves show the approximation (5.12); at $b/h = 0.8$ the approximation is an overestimate by about 20% (see figure 8*b*).

Here, $M(B/\pi)$ is the function defined in (4.7) and (4.13), and shown in figure 4. It is interesting that both the physical ridge height, b, and the WKB height, B in (5.2), appear in (5.12).
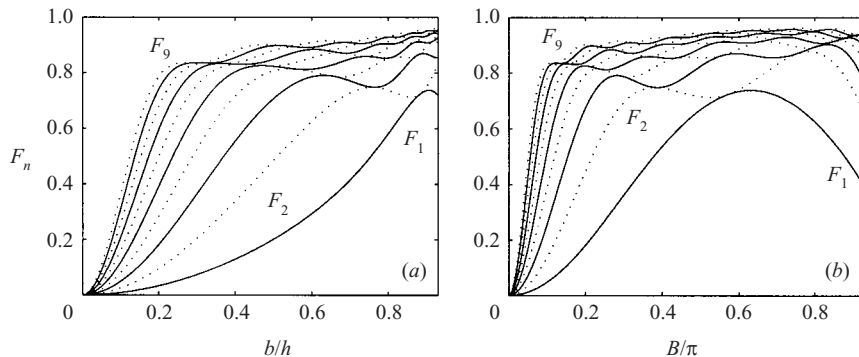
FIGURE 7. Fraction of the converted energy in the first n modes for the HOTS profile. (Compare with figure 5, which shows F_n for uniform stratification.)
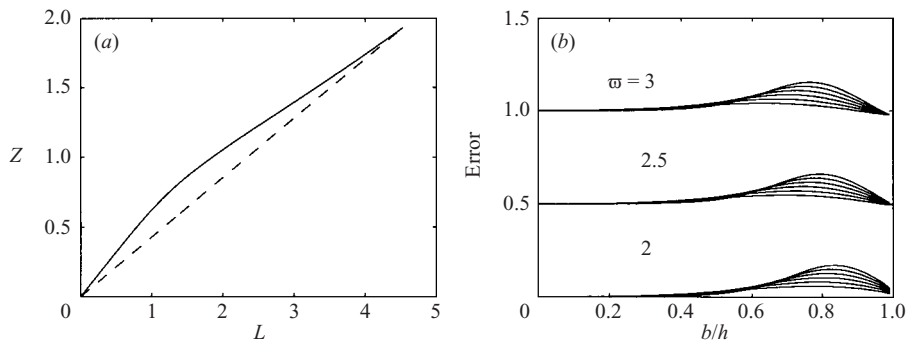

FIGURE 8. (a) A comparison using the HOTS profile of the approximation (5.10) (the dashed line) with the exact $L(Z)$ (the solid curve). (b) The error defined in (5.13) as a function of b/h for $\varpi \equiv \bar{N}/\mathcal{N}_B = 2$, 2.5 and 3, and $\beta \equiv h/d = 5$, 6, ..., 10. The curves corresponding to different values of ϖ are vertically offset by 0.5. The maximum error of about 20% occurs at $b/h \approx 0.8$.

Figure 8(b) compares the approximation (5.12) with a numerical solution of (5.1) using

$$\text{Error} \equiv \frac{\text{approximate } \mathscr{C}}{\text{numerical } \mathscr{C}} - 1. \tag{5.13}$$

The approximation overestimates $\mathscr{C}$ by up to 20% when $b/h \approx 0.8$. A further assessment of (5.12) is the comparison between the solid (numerical) and dashed (approximation) curves in figure 6(c) (this is a worst case because $b/h = 0.8$).

6. Conclusion

We conclude by using (5.4) to make a numerical estimate using values representative of the Hawaiian ridge:

$$(b, h) = (4500, 5000)\,\text{m}, \quad f = 5 \times 10^{-5}\,\text{s}^{-1}. \tag{6.1}$$

For the tidal velocity away from the ridge we take $U = 0.01\,\text{m s}^{-1}$. With the WOD

data in table 1, $\bar{N} = 1.02$ c.p.h. and so the dimensional prefactor in (5.4) is then

$$\mathscr{C}_\star \equiv \rho_0 U^2 \bar{N} \sqrt{1 - \frac{f^2}{\omega^2} \frac{h^2}{\pi^2}},$$

$$\approx 4.2 \times 10^2 \, \text{W m}^{-1}. \tag{6.2}$$

With the WOD profile the numerical solution of (5.4) and (5.5) gives $K = 19.7$ so that if we take the length of the ridge to be $L = 2000$ km then

$$\mathscr{C}_{\text{WOD}} \approx \mathscr{C}_\star \times K \times L = 16.6 \, \text{GW}. \tag{6.3}$$

The HOTS profile has $\bar{N} = 1.22$ so that $\mathscr{C}_\star$ is larger by 20%. But because of the details in K, the final result for $\mathscr{C}_{\text{HOTS}}$ is very close to $\mathscr{C}_{\text{WOD}}$ (see table 1).

It is interesting to compare (6.3) with a value obtained by assuming a uniformly stratified ocean with $N = 1$ c.p.h. (close to the observed $\bar{N}$ for WOD). With $b/h = 0.9$, we have for a uniformly stratified ocean $K \approx 11.72$ and so $\mathscr{C} = 4.9$ GW. This is smaller than (6.3) because the estimate has taken no account of the stronger stratification at the ridge.

St. Laurent *et al.* (2003) use the same knife-edge model, but with a uniform buoyancy frequency $N = 2.8$ c.p.h. Additionally they take $L = 2000$ km, $U = 0.014 \, \text{m s}^{-1}$, and $b/h = 0.75$; the resulting estimate is $\mathscr{C} \approx 19$ GW. The differences between our values for L, U, and N and those of St. Laurent *et al.* (2003) give some indication of the subjective choices which must be made in applying the knife-edge model to the complicated three-dimensional geometry of the Hawaiian Ridge. The jagged profile of the Hawaiian Ridge is a major source of uncertainty in these estimates. This is a strong motivation for studying the three-dimensional problem of a knife-edge with variable height.

It is also of interest to compare (6.3) with observational and numerical estimates of $\mathscr{C}$. Using an inverse model constrained with TOPEX data, Egbert & Ray (2000, 2001) estimate that the total M_2 conversion at Hawaii is 20 GW. Simulations using the Princeton Ocean model predict that the tidal conversion occurring at Hawaii is 9.7 GW (Merrifield, Holloway & Shaun Johnston 2001; Merrifield & Holloway 2002). Ray & Mitchum (1996) estimated 15 GW of conversion into the first baroclinic mode. To put these numbers into global perspective, Munk & Wunsch (1998) estimate that the total amount of energy radiated into the internal gravity wave field by tidal interaction with with deep-ocean ridges and seamounts is 900 GW.

The knife-edge ridge is the simplest tractable model of internal tide generation by strongly supercritical topography. Using this idealization we have found two mechanisms which increase the conversion by orders of magnitude above earlier results obtained using models with uniform stratification and infinite depth. First, as the gap width $h - b$ is reduced the conversion becomes infinite with $\mathscr{C} \propto \ln[(h-b)/h]$ (see (4.10) with $\tau \gg 1$). The second factor which greatly effects $\mathscr{C}$ is the structure of the buoyancy frequency, $N(z)$. The factor $N(b)$ in (5.12) indicates the strong dependence of the conversion rate on stratification if the ridge penetrates the thermocline.

REFERENCES

Baines, P. G. 1973 The generation of internal tides by flat-bump topography. *Deep-Sea Res.* **20**, 19–205.

Baines, P. G. 1982 On internal tide generation models. *J. Phys. Oceanogr.* **29**, 307–382.

Balmforth, N. J., Ierley, G. R. & Young, W. R. 2002 Tidal conversion by subcritical topography. *J. Phys. Oceanogr.* **32**, 2900–2914.

Bell, T. H. 1975a Lee waves in stratified fluid with simple harmonic time dependence. *J. Fluid Mech.* **67**, 705–722.

Bell, T. H. 1975b Topographically generated internal waves in the open ocean. *J. Geophys. Res.* **80**, 320–327.

Carrier, G. F., Krook, M. & Pearson, C. E. 1983 *Functions of a Complex Variable*. Ithaca, New York: Hod Books.

Conkright, M. E., Antonov, J. I., Baranova, O., Boyer, T. P., Garcia, H. E., Gelfeld, R., Johnson, D., Locarnini, R. A., Murphy, P. P., O'Brien, T. D., Smolyar, I. & Stephens, C. 2001 *World Ocean Database 2001*, *NOAA Atlas NESDIS*, vol. 1. Washington, DC: US Government Printing Office.

Egbert, G. D. & Ray, R. D. 2000 Significant dissipation of tidal energy in the deep ocean inferred from satellite altimeter data. *Nature* **405**, 775–778.

Egbert, G. D. & Ray, R. D. 2001 Estimates of M_2 tidal energy dissipation from TOPEX/Poseidon altimeter data. *J. Geophys. Res.* **106**, 22 475–22 502.

Fowkes, N. & Silberstein, J. P. O. 1995 John Joseph Mahoney 1929–1992. *Historical Records of Australian Science* **10** (3), see also http://www.science.org.au/academy/memoirs/mahony.htm.

Holloway, P. E. & Merrifield, M. A. 1999 Internal tide generation by seamounts, ridges and islands. *J. Geophys. Res.* **106**, 22 475–22 502.

HOTS 2002 Hawaii ocean time-series program. Data available online at http://hahana.soest.hawaii.edu/hot/hot_jgofs.html.

Hurley, D. G. 1997 The generation of internal waves by vibrating elliptic cylinders. Part 1. Inviscid solution. *J. Fluid Mech.* **351**, 105–118.

Khatiwala, S. 2003 Generation of internal tides in an ocean of finite depth: analytical and numerical calculations. *Deep-Sea Res.* I **50**, 3–21.

Larsen, L. H. 1969 Internal waves incident upon a knife edge barrier. *Deep-Sea Res.* **16**, 411–419.

Ledwell, J. R., Montgomery, E. T., Polzin, K. L., St. Laurent, L. C., Schmitt, R. W. & Toole, J. M. 2000 Evidence of enhanced mixing over rough topography in the abyssal ocean. *Nature* **403**, 179–182.

Li, M. 2003 Energetics of internal tides radiated from deep-ocean topographic features. *J. Phys. Oceanogr.* (submitted).

Llewellyn Smith, S. G. & Young, W. R. 2002 Conversion of the barotropic tide. *J. Phys. Oceanogr.* **32**, 1554–1566.

Merrifield, M. A. & Holloway, P. E. 2002 Model estimates of M_2 internal tide energetics at the Hawaiian Ridge. *J. Geophys. Res.* **107**, C8, 10.1029/2001JC000996.

Merrifield, M. A., Holloway, P. E. & Shaun Johnston, T. M. 2001 The generation of internal tides at the Hawaiian Ridge. *Geophys. Res. Lett.* **28**, 559–562.

Munk, W. H. & Wunsch, C. I. 1998 Abyssal recipes II: energetics of tidal and wind mixing. *Deep-Sea Res.* **45**, 1977–2010.

Ray, R. D. & Mitchum, G. D. 1996 Surface manifestation of internal tides generated near Hawaii. *Geophys. Res. Lett.* **23**, 2101–2104.

Robinson, R. M. 1969 The effects of a barrier on internal waves. *Deep-Sea Res.* **16**, 421–429.

St. Laurent, L. C. & Garrett, C. 2002 The role of internal tides in mixing the deep ocean. *J. Phys. Oceanogr.* **32**, 2882–2899.

St. Laurent, L. C., Stringer, S., Garrett, C. & Perrault-Joncas, D. 2003 The generation of internal tides at abrupt topography. *Deep-Sea Res.* I **50**, 987–1003.

Tuck, E. O. 1980 Application and solution of Cauchy-singular integral equations. In *The Application and Numerical Solution of Integral Equations* (ed. R. S. Anderssen, F. R. de Hoog & M. A. Lukas), pp. 21–50. Alphen aan den Rijn: Sijthoff and Noordhoff.

Wunsch, C. 1975 Internal tides in the ocean. *Rev. Geophys.* **13**, 167–182.